Analytical Methods

ROYAL SOCIETY OF CHEMISTRY

PAPER

View Article Online
View Journal | View Issue

Cite this: *Anal. Methods*, 2025, **17**, 2263

Chemical profiling of surviving cancer cells using ToF-SIMS and MCR analysis discriminates cell components†

Auraya Manaprasertsak, [abc] Robin Rydbergh, [d] Qicheng Wu, [abc] Maria Slyusarenko, [abc] Christopher Carroll, [abc] Sarah R. Amend, [e] Sofie Mohlin, [bcf] Kenneth J. Pienta, [e] Per Malmberg [d] and Emma U. Hammarlund *[abc]

Cancer cells survive treatment through mechanisms that remain unclear. This study investigates the chemical changes that occur in cancer cells after treatment, focusing on lipid metabolism as a potential marker for survival and resistance. Using Time-of-Flight Secondary Ion Mass Spectrometry (ToF-SIMS) and advanced multivariate statistical analysis, we compared the chemical profiles of untreated and surviving cancer cells. Region-of-Interest (ROI) analysis revealed distinct differences in the lipid compartments, with surviving cancer cells showing significant accumulation of lipid droplets. While Principal Component Analysis (PCA) was able to differentiate the chemistry of untreated and surviving cancer cells as well as their cellular components, Multivariate Curve Resolution (MCR) provided a clearer and more detailed distinction, enabling the identification of specific cellular features such as the cytoplasm, nucleus, and lipid droplets within the surviving cells. The separation of the chemistry in nucleus and lipid droplets emphasizes the effectiveness in complex spectral analysis. Furthermore, the ability to map the distribution of lipid droplets in surviving cells can advance our understanding of how these structures contribute to cancer cell survival during treatment. The study highlights the importance of lipid droplets as potential biomarkers for cancer cell adaptation and survival post-treatment, with implications for developing new therapeutic strategies.

Received 12th December 2024
Accepted 9th February 2025

DOI: 10.1039/d4ay02238f

rsc.li/methods

Introduction

Chemical signatures play a crucial role in tracing diseases,[1,2] including cancer, beyond the scope of traditional genetic mutations. Various studies have shown how cancer affects the chemistry of elements and their isotopes. For example, tumor growth and metastasis have been linked to increased copper requirements.[3] This suggests the potential of high-precision metal isotope analysis to enhance our understanding of cancer and its biochemical pathways.[4] Alteration to the composition of stable isotope elements including carbon, nitrogen, and sulfur have been demonstrated to indicate the presence of breast cancer[5] and endometrial cancer.[6] In addition, the cholesterol profile has been demonstrated to be altered in cancer tissues.[7] These findings collectively demonstrate the potential of chemical signatures as powerful tools for unraveling the complexities of cancer biology.

Mapping the distribution and properties of molecules of tissues and cells requires mass spectrometry (MS) methods.[8–10] MS has proven effective in bulk analysis of chemistry in tissues,[11,12] blood,[13] and cells,[14,15] revealing disease-specific chemical alterations. Although the analyses can map the distributions in tissue samples, such as lipids and fatty acids in breast cancer[16] and glioma tissues,[17,18] only a few studies have utilized MS to map the chemistry at the cellular level including subcellular imaging of snow algae.[19] Since the spatial resolution of most MS techniques is at the boundary of being able to track the chemical composition in a typically sized human cell, *i.e.*, approximately 20 μm.[20]

Cellular spatial chemical mapping offers immense potential for enhancing our understanding of cancer but also presents significant challenges. Matrix-Assisted Laser Desorption/Ionization Mass Spectrometry (MALDI-MS), which generally provides a spatial resolution of around 10–20 μm, may lack the precision needed to capture fine cellular structures in detail.[21,22]

[a]*Department of Experimental Medical Science, Lund University, Lund, Sweden. E-mail: emma.hammarlund@med.lu.se*
[b]*Lund University Cancer Center, Lund University, Lund, Sweden*
[c]*Lund Stem Cell Center, Lund University, Lund, Sweden*
[d]*Department of Chemistry and Chemical Engineering, Chalmers University of Technology, Gothenburg, Sweden*
[e]*The Cancer Ecology Center, Brady Urological Institute, Johns Hopkins School of Medicine, Baltimore, MD, USA*
[f]*Division of Pediatrics, Department of Clinical Sciences, Lund University, Lund, Sweden*

† Electronic supplementary information (ESI) available. See DOI: https://doi.org/10.1039/d4ay02238f

In contrast, techniques like Time-of-Flight Secondary Ion Mass Spectrometry (ToF-SIMS) and Nanoscale Secondary Ion Mass Spectrometry (NanoSIMS) offer significantly higher spatial resolution, ranging from submicron to nanometer scales, allowing researchers to visualize molecular distributions at the subcellular level with remarkable clarity.[22,23] While NanoSIMS is limited to molecules that are labelled with stable isotope, ToF-SIMS is particularly valuable when examining the distribution of molecules within cancer cells.[24,25] Orbitrap Secondary Ion Mass Spectrometry (Orbi-SIMS), despite its slightly lower lateral resolution (2 μm), has demonstrated potential in cancer research due to its high mass resolution. For instance, it has been used to distinguish metabolic profiles between tumor and stromal cells in murine cancer models, complementing existing spatial imaging methods.[26] In response to environmental stressors like chemotherapy, surviving cancer cells exhibit larger nuclei and cell sizes.[27] Since these cells play critical roles in cancer progression, therapeutic resistance, and recurrence, it is key to understand their survival mechanisms.[28] By mapping the chemical differences between untreated cancer cells and those that have survived cisplatin treatment, spatial mapping *via* mass spectrometry has the potential to shed new light on chemical and biological changes.

In this study, we investigate whether ToF-SIMS can reliably map the chemical distribution across different cellular components of cancer cells that survive treatment. Surviving cancer cells refer to those that remain viable following therapy, while untreated cancer cells represent the control population that has not been exposed to any therapeutic intervention. Here, by analyzing the chemical profiles of both treated and untreated cells, we aim to identify specific molecular differences associated with treatment resistance. We evaluate the performance of two advanced analytical techniques, principal component analysis (PCA) and multivariate curve resolution (MCR), in distinguishing between these two cell populations. Our results contribute to a deeper understanding of the chemical alterations that enable cancer cells to survive treatment.

Materials and methods

Cell culture

HCC-1806 breast cancer cells were obtained from ATCC and cultured in DMEM GlutaMAX (Thermo Fisher Scientific, Sweden), supplemented with 10% FBS (Thermo Fisher Scientific, Sweden), without penicillin/streptomycin. All cells were maintained in a humidified incubator at 37 °C with 5% CO_2.

Treatment

The experiment involved three distinct cell sample types:

(1) Untreated cancer cells: HCC-1806 cells were cultured under standard conditions without cisplatin treatment and reseeded on cover slips for 24 hours.

(2) Surviving cancer cells: HCC-1806 cells (2×10^6 per T75 flask) were seeded overnight and treated with cisplatin at LD_{50} (3 μM) for 72 hours (defined as the day 0 timepoint). The culture media was refreshed every 3–4 days. By day 10, surviving cells exhibiting enlarged polyaneuploid characteristics were trypsinized, size-filtered using a 10 μm mesh filter (Nordic Diagnostica, Sweden), and reseeded on cover slips for 24 hours.

(3) Mixed untreated and surviving cancer cells: a mixture of untreated and surviving HCC-1806 cells were reseeded together on the same cover slips for 24 hours.

Sample preparation

For ToF-SIMS analysis, all samples were prepared as follows: the culture medium was aspirated from each cover slip, followed by three washes with phosphate-buffered saline (PBS) (Fisher Scientific, Sweden) and three additional washes with 0.15 M ammonium acetate (Sigma-Aldrich, Sweden) at pH 7.4 (adjusted with ammonia solution). Cover slips were then rapidly dipped in isopropanol and flash-frozen in liquid nitrogen. Prepared samples were stored at −80 °C until further analysis.

ToF-SIMS analysis

Prior to the ToF-SIMS analysis, all cover slips were placed on pre-cooled metal blocks and dehydrated using a freeze-dryer (Christ Alpha 1-2 LDplus, Germany) to remove water while preserving the biological structure by gradually adjusting the temperature. The ToF-SIMS measurements were then conducted at room temperature under high vacuum conditions using a top-mount sample holder. The samples were investigated using a ToF-SIMS V (ION-TOF, Munster, Germany), equipped with a bismuth (Bi_3) liquid metal ion gun (LMIG) as a primary ion source (30 keV for Bi_3^+ and 60 keV for Bi_3^{++}) and an Ar-gas cluster ion beam (GCIB) (5 keV) as a sputtering beam. The current was approximately 0.4 pA in spectrometry mode with an ion dose of 5×10^{12} ions per cm^2, and 0.1 pA in the delayed extraction mode (DEEX) with an ion dose of 1×10^{12} ions per cm^2. Both ion doses are below the static limit of 10^{13} ions per cm^2, ensuring that the surface molecular information remains intact and minimizing surface damage during the analysis. In spectrometry mode, the ToF-SIMS spectra of untreated and surviving cancer cells were recorded separately in positive mode and negative mode in total of 100 scans across three replicates. The 100×100 μm^2 FoV areas were measured by the Bi_3^{++} gun at 60 keV in a 1 shot per frame per pixel random mode raster to produce a 128 × 128 pixels frame together with a non-interlaced (1 s sputter, 0.5 s pause). In DEEX mode, the ToF-SIMS spectra and images of the mix of untreated and surviving cancer cells were recorded in negative mode in total of 180 scans across three replicates. The 220×220 μm^2 FoV areas were measured by the Bi_3^{++} gun at 60 keV to produce a 256 × 256 pixels raster in random mode with 2 shot per frame per pixel, together with a non-interlaced (1 s sputter, 0.5 s pause) Ar_{1500}^+ GCIB sputter at 5 keV and 3.09 nA current to sputter a raster crater of 400×400 μm^2. All ToF-SIMS spectra and images were analyzed with the Surface Lab software (version 7.3; ION-TOF, GmbH). The mass spectra were internally calibrated to signals of $[C]^+$, $[CH]^+$, $[CH_2]^+$, $[CH_3]^+$, and $[C_{27}H_{45}]^+$ in the positive ion mode and $[C]^-$, $[CH]^-$, $[OH]^-$, $[F]^-$, and $[CN]^-$ in the negative mode. The achieved mass resolution, exemplified

by the $[CN]^-$ peak at m/z 26, was approximately 6500 (FWHM) in the negative ion mode.

Multivariate analysis of negative images

The peak search function in SurfaceLab software (version 7.3; ION-TOF, GmbH) was applied to spectra from each region of interest (ROI). Peaks within the m/z 10–420 range that had counts exceeding 100, a signal-to-noise ratio (SNR) greater than 1, and a peak width of 0.8 Da were selected. For the analysis, three replicate measurements from 30 × 30 μm^2 of four ROI spectra of cancer cells were used. The dataset included 190 negative ions, which were then subjected to Principal Component Analysis (PCA) and Partial Least Squares Discriminant Analysis (PLS-DA) using MATLAB. In the analysis of ToF-SIMS image data, both PCA and Multivariate Curve Resolution (MCR) were performed using the Multivariate Statistical Analysis (MVSA) function in SurfaceLab software. The peaks within the full mass range that had counts exceeding 100, a SNR greater than 1, and a peak width of start at 1, end at 6 ns were selected. Both PCA and MCR were applied to 2D ToF-SIMS images using six factors, selected as optimal for distinguishing chemical variations. No XY binning (without averaging adjacent data points) was used, and variance spectral scaling was applied to enhance feature differentiation and improve the interpretation of chemical distributions.

Results and discussion

Surviving cancer cells and untreated cancer cells

To map the chemical distribution of untreated and surviving breast cancer cells, HCC-1806 cells were treated with cisplatin for 72 hours. By day 10, surviving cells exhibited the enlarged cell size characteristics typical of endocycling cancer cells.[27] As visualized by phase contrast microscopy, treated HCC-1806 cells presented a substantial increase in cell body size (Fig. 1). The diameter of adherent surviving cancer cells is approximately 10 times larger than that of untreated cells.[27] Along with the increase in overall cell size, we also observed a significant enlargement of the nuclei within surviving cells.[29,30] Additionally, structural features, such as peroxisomes or lipid droplets, appeared more prominent in the surviving cells compared to the untreated cells, suggesting a potential connection between these organelle changes and the survival mechanisms in these cells.[31–33]

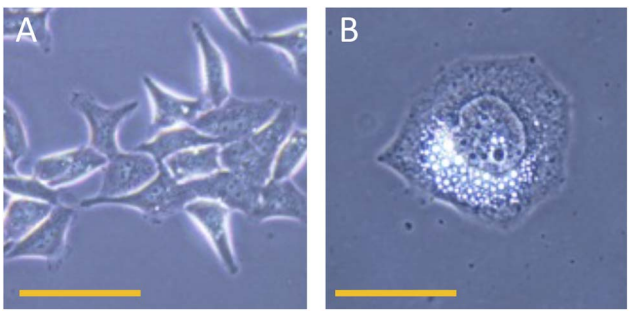

Fig. 1 Detailed view of (A) untreated HCC-1806 breast cancer cell and (B) surviving HCC-1806 breast cancer cell 10 days post-treatment using phase contrast microscopy. The scale bar is 100 μm.

Spectrometry mode ToF-SIMS analysis

We initiated our analysis by separately examining untreated cancer cells and surviving cancer cells using ToF-SIMS in both positive and negative ion modes. By using a lower GCIB acceleration voltage, we optimized lipid signal detection while minimizing fragmentation.[23] This approach allowed us to capture a comprehensive chemical profile of both cell populations, providing insight into their molecular composition and potential differences in their chemical distributions.

In the positive ion mode, where the instrument detects positively charged ions generated from the sample, both untreated cancer cells and surviving cancer cells exhibited a prominent cholesterol peak at m/z 369.3 ($C_{27}H_{45}^+$) (Fig. 2), which is consistent with the known cholesterol ion signal.[12,34] Cholesterol plays a critical role in processes such as maintaining membrane structure and cell signaling, both in healthy and cancer cells.[35] Additionally, a phosphatidylcholine (PC) headgroup at m/z 184.1 ($C_5H_{15}NO_4P^+$) and with one molecule of water (m/z 18.0) removed at m/z 166.1 ($C_5H_{13}NO_3P^+$) were observed[36] (Fig. S1†). However, distinct differences in peak intensities and patterns were observed in the mass spectra—representing the abundance of ions at various mass-to-charge (m/z) ratios—between untreated and surviving cancer cells within the m/z 400–600 range (Fig. 2). The surviving cancer cells exhibited prominent peaks corresponding to monoacylglycerol (MAG) lipids in the m/z 300–350 range and diacylglycerol (DAG) lipids in the m/z 500–600 range.[12,37] In contrast, these lipid patterns were absent in the spectra from untreated cancer cells. This difference suggests potential alterations in lipid metabolism, particularly in lipid signaling pathways, in the surviving cancer cells.

In the negative ion mode, both untreated and surviving cancer cells exhibited characteristic fatty acid peaks, including FA (16 : 0) at m/z 255.2 ($C_{16}H_{31}O_2^-$), FA (18 : 1) at m/z 281.2 ($C_{18}H_{33}O_2^-$), and FA (18 : 0) at m/z 283.2 ($C_{18}H_{35}O_2^-$).[38,39] These fatty acids are integral components of phospholipids that make up the cellular membrane and lipid droplets within the cytoplasm. Only the surviving cancer cells showed peaks corresponding to PC 16 : 0/18 : 1 at m/z 419.3 ($C_{21}H_{40}PO_6^-$)[40] and epoxidized phosphatidylcholine (PC) 16 : 0/18 : 1 at m/z 473.2 ($C_{29}H_{45}O_5^-$) and m/z 489.2 ($C_{29}H_{45}O_6^-$).[41] These specific phospholipid peaks were absent in the untreated cancer cells, suggesting that the surviving cells underwent lipid modifications, potentially related to stress response or adaptation mechanisms following treatment. The presence of epoxidized PC may indicate oxidative stress or altered phospholipid metabolism,[42] which could be crucial for the survival and persistence of these cells (Fig. 3).

Delayed extraction mode ToF-SIMS analysis

To ensure consistent analytical conditions across all ToF-SIMS analyses, we employed delayed extraction mode for the

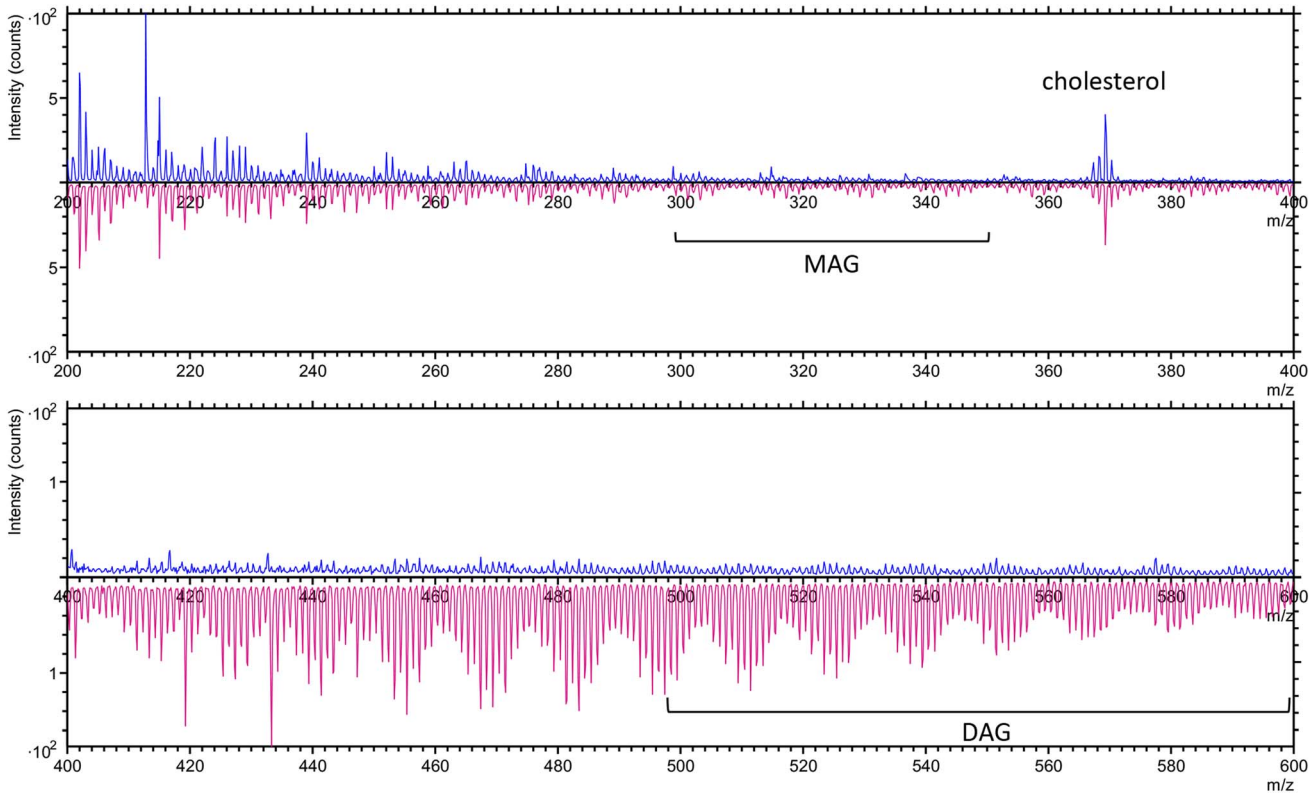

Fig. 2 The overlay spectra of untreated cancer cells (blue) and surviving cancer cells (pink) in positive ion mode in the range of *m/z* 200–400 (upper panel) and 400–600 (lower panel).

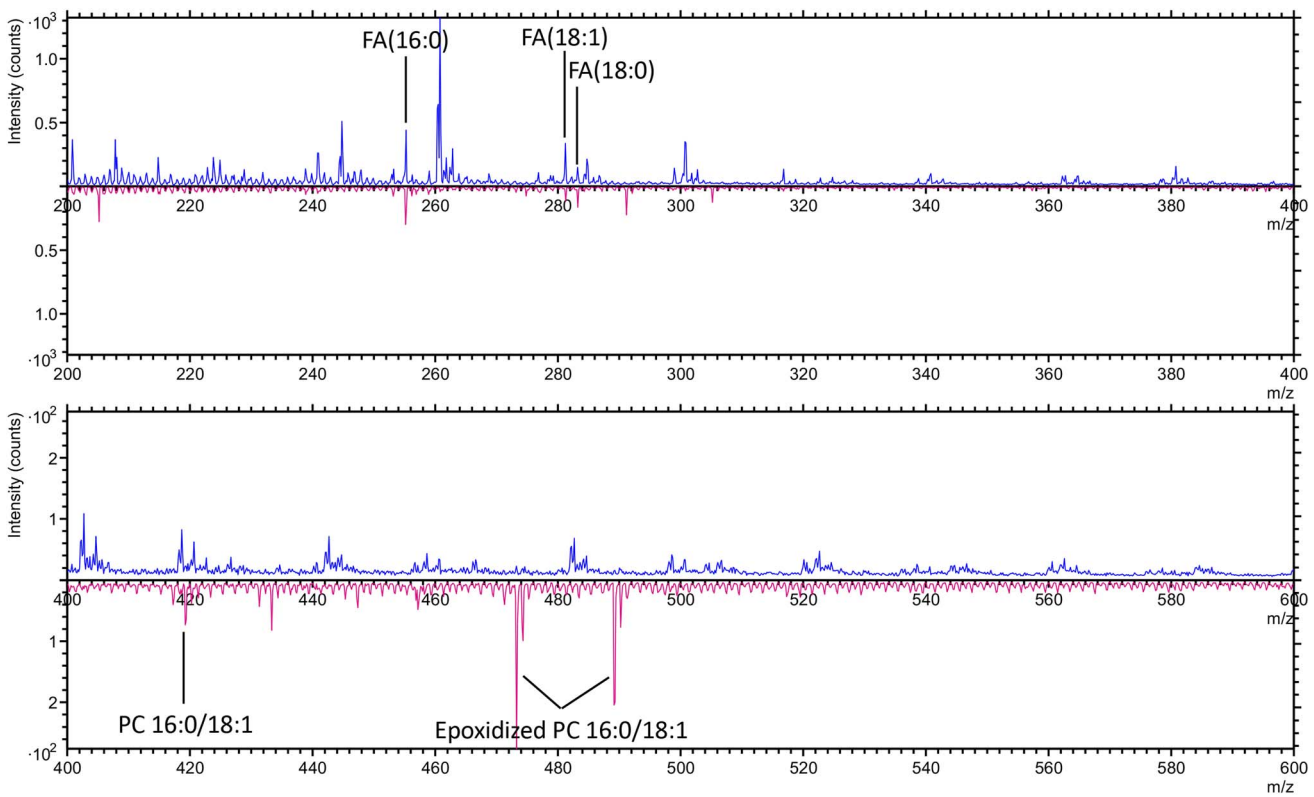

Fig. 3 The overlay spectra of untreated cancer cells (blue) and surviving cancer cells (pink) in negative ion mode in the range of *m/z* 200–400 (upper panel) and 400–600 (lower panel).

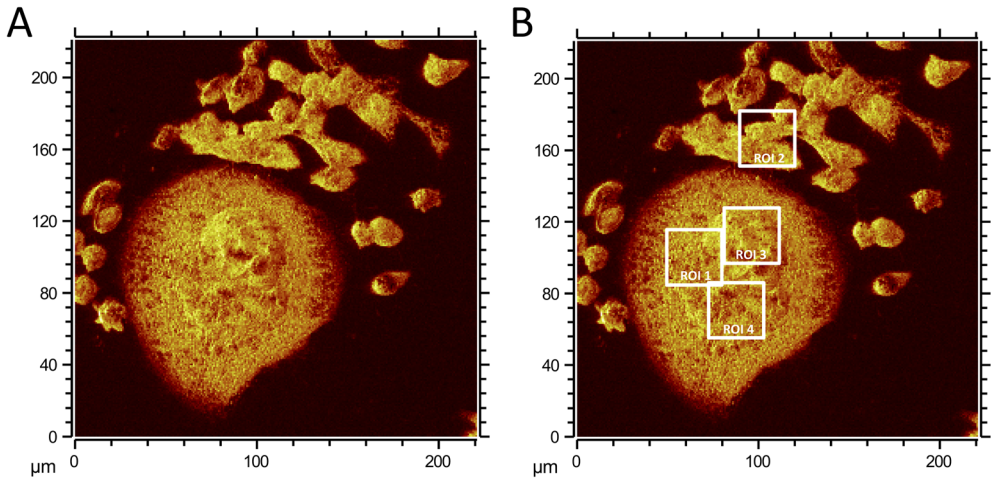

Fig. 4 The ToF-SIMS images from negative ion mode of a mixed of cells that are untreated (small) and surviving cancer cells (large): (A) total ion and (B) total ion with four regions of interests (ROI1-4).

investigation of both untreated and surviving cancer cells. By seeding both cell types on the same coverslip (Fig. 4A), we minimized variability in sample preparation and environmental factors, thereby enhancing the reliability of our comparisons. The analysis was conducted in negative ion mode, which is optimal for detecting relevant fatty acid signals in cancer cells.[43]

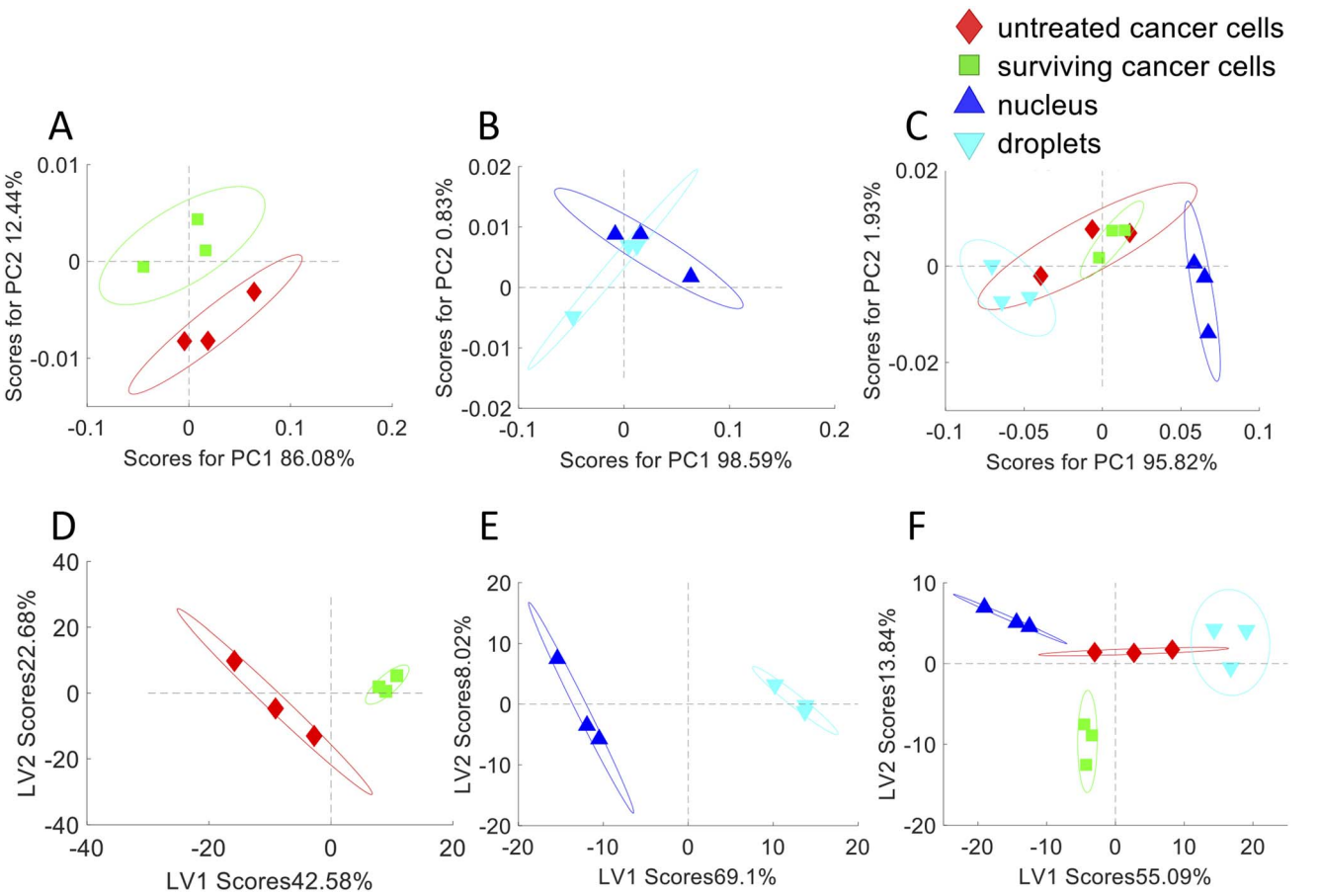

Fig. 5 Dimensionality reduction and discriminant analysis of negative spectra from cancer cells regions: PCA of negative spectra from (A) untreated and surviving cancer cells, (B) the nucleus and lipid droplets of surviving cancer cells, and (C) untreated cancer cells, surviving cancer cells, the nucleus from surviving cancer cells, and lipid droplets from surviving cancer cells. PLS-DA of negative spectra from (D) untreated and surviving cancer cells, (E) the nucleus and lipid droplets of surviving cancer cells, and (F) untreated cancer cells, surviving cancer cells, the nucleus from surviving cancer cells, and lipid droplets from surviving cancer cells.

For detailed analysis, we applied ROI extraction, selecting specific regions within the image. We defined 30 × 30 μm^2 ROIs for untreated (ROI 1) and surviving (ROI 2) cancer cells (Fig. 4B) and performed PCA and PLS-DA on their negative ion spectra using MATLAB.

The PCA and PLS-DA analysis using MATLAB revealed a clear separation between untreated (ROI 2, Fig. 4B) and surviving (see ROI 1, Fig. 4B) cancer cells (Fig. 5A and D). This separation indicates that each cell type has its distinct chemical profiles. Further analysis was conducted on two key components within the surviving cancer cells, which were identified as likely representing the nucleus (ROI 3, Fig. 4B) and lipid droplets (ROI 4, Fig. 4B). PCA and PLS-DA of these regions demonstrated clear separation as well (Fig. 5B and E). This separation suggests unique chemical compositions between the nucleus and lipid droplets, potentially linked to their roles in therapeutic resistance and cellular adaptation. To further validate and refine the interpretation of these findings using limited regions of interest, we proceeded with multivariate statistical analysis (MVSA) using spectra from the entire negative ion images.

Imaging MVSA of ToF-SIMS data

In this study, negative ion images of the mixed untreated and surviving cancer cells sample from ToF-SIMS were analyzed using MVSA *via* the SurfaceLab software. As opposed to the ROI-approach, MVSA analyses uses spectra from the entire image. This data can be binned into factors that represents different groups of molecules. Using this data, we first applied PCA followed by MCR. PCA with six factors (F1–F6) was initially performed to explore potential differences between untreated and surviving cancer cells. PCA was able to distinguish some differences between the two cell types and identify distinctions between components such as lipid droplets and the nucleus, but it did not clearly separate the cytoplasm (Fig. 6). PCA is inherently limited in its ability to classify overlapping chemical profiles, as its primary function is to reduce data dimensionality rather than to specifically separate chemical components.

In contrast, MCR with six factors provided a much clearer separation, effectively distinguishing between untreated and surviving cancer cells and resolving major components within the surviving cells, including the cytoplasm, nucleus, and lipid droplets (Fig. 7). MCR is specifically developed to handle this complexity by separating pure spectra and their associated concentration profiles. Indeed, MCR was able to decompose the spectral data into F1, F3, and F5, represents distinct chemical profiles between these regions (Fig. 7).

From F1, F3, and F5 of the MCR analysis, we identified three major components in the surviving cells. We examined the peaks with the highest loadings (Table S1†) in each of these factors to determine their potential to represent specific cell structures: the nucleus (F1), lipid droplets (F3), and cytoplasm (F5), respectively.

From F1, we saw the high loadings from phosphate groups at *m*/*z* 62.9 (PO_2^-), 78.9 (PO_3^-), and 158.9 ($P_2O_6H^-$)[44] and the cytosine (N-base) at *m*/*z* 134.1 ($C_4H_5N_3O^-$). Since phosphates

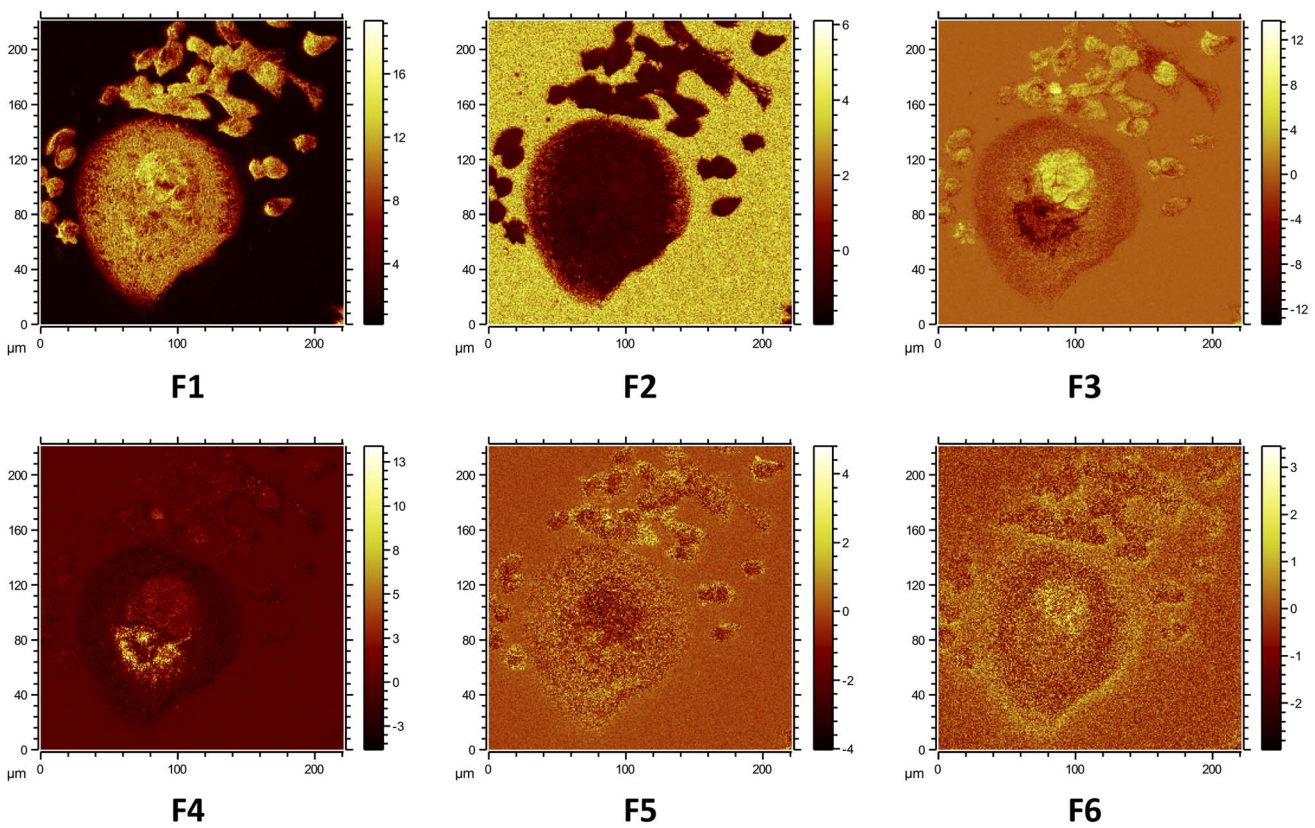

Fig. 6 The six factors (F1–F6) of PCA analysis from negative ion images which untreated and surviving cancer cells are mixed.

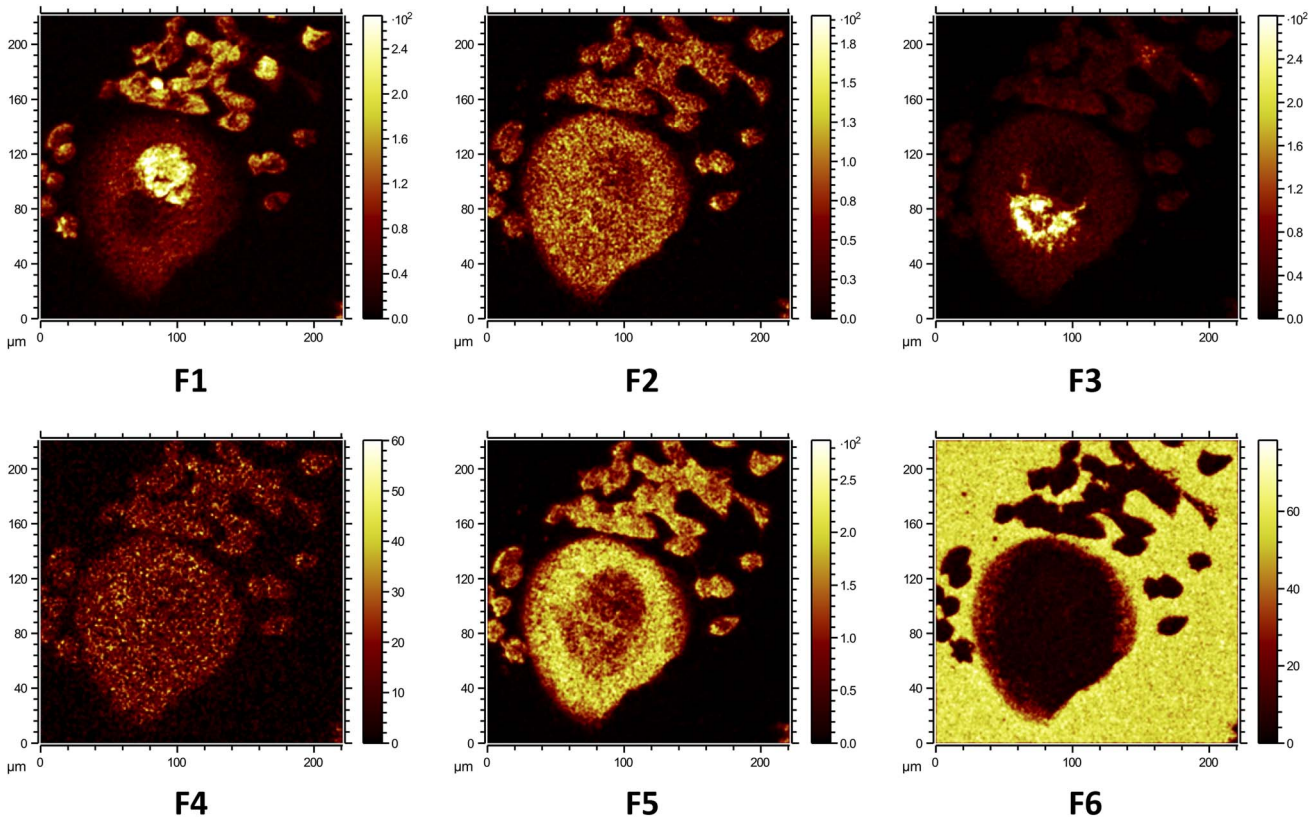

Fig. 7 The six factors (F1–F6) of MCR analysis from negative ion images which untreated and surviving cancer cells are mixed.

and nitrogenous bases are a major component of DNA and RNA backbones,[45] their presence is likely indicative of nucleotide being detected within the nucleus.[46]

From F3, we found the loadings at *m*/*z* 45.0 (CH_3NO^-), 100.0 ($C_4H_6NO_2^-$) that typically correspond to a fragment from amino acids.[47] This could point to alterations in protein or amino acid metabolism, which are commonly observed in cancer cells undergoing stress or adapting to treatments.[48] Loadings at *m*/*z* 59.0 ($C_2H_3O_2^-$), 71.0 ($C_3H_3O_2^-$), 73.0 ($C_3H_5O_2^-$), and 87.0 ($C_4H_7O_2^-$), that indicated carboxylate-containing molecules, potentially from fatty acids or lipid degradation products. This may reflect the fragmentation of stored lipids, particularly from fatty acids or glycerol-based lipids. Loading at *m*/*z* 113.0 ($C_5H_5O_4^-$) corresponds to citrate fragment.[49] Citrate metabolism is often dysregulated in cancer cells, which tend to exhibit altered energy production pathways (*e.g.*, the Warburg effect).[50] In addition, citrate metabolism may be altered to meet the demands for biosynthesis and rapid proliferation in cancer cells.

From F5, we saw high loading of *m*/*z* 26.0 (CN^-) and 42.0 (CNO^-). Molecules with these masses are often detected in cell and tissue samples,[25] particularly in environments with rich nitrogenous compounds. These molecules can originate from amino acids, proteins, peptides, nucleic acids, or other nitrogen-containing biomolecules commonly found in all part of cells as the distribution in F2. We also found the loading at *m*/*z* 97.0 (HSO_4^-) which indicates sulfur-containing metabolites within the cytoplasm.[51] Moreover, there was the loading at *m*/*z* 94.9 (PO_4^-) and at *m*/*z* 129.1 ($C_3H_6PO_4^-$) in F4 which are often from phospholipids from phospholipid metabolism. Phospholipids are a major component of the cellular and organelle membranes within the cytoplasm.[52]

The improved performance of MCR in comparison to PCA can be attributed to several factors. While PCA identifies variance in the data by capturing orthogonal components, it may not always capture subtle or nonlinear patterns, especially when the dataset involves overlapping chemical signals or complex biological variations.[53] MCR, however, is specifically designed to address such complexity by extracting pure spectra and concentration profiles, thereby minimizing residuals between the original and reconstructed data.[54] This capability allows MCR to separate overlapping chemical profiles effectively, even in intricate environments, making it especially suitable for ToF-SIMS imaging analysis of cells.[55] This allows MCR to better separate the molecular signatures of untreated and surviving cancer cells, as well as the distinct components within the surviving cells, such as the nucleus and lipid droplets (Fig. 8C).

The identification of lipids is particular interest since lipid droplets have previously been associated to an increased capacity to handle reactive oxygen species in surviving cancer cells.[31,33] However, lipid droplets may also confer an advantage related to the diffusion of oxygen. Oxygen diffusion is inversely correlated to distance, which means that diffusion of oxygen into large surviving cells should be negatively affected as compared to the rate in untreated cells. However, oxygen diffuses faster in lipids than in aqueous solutions.[56] We therefore ask if the presence of lipid droplets could facilitate intra-

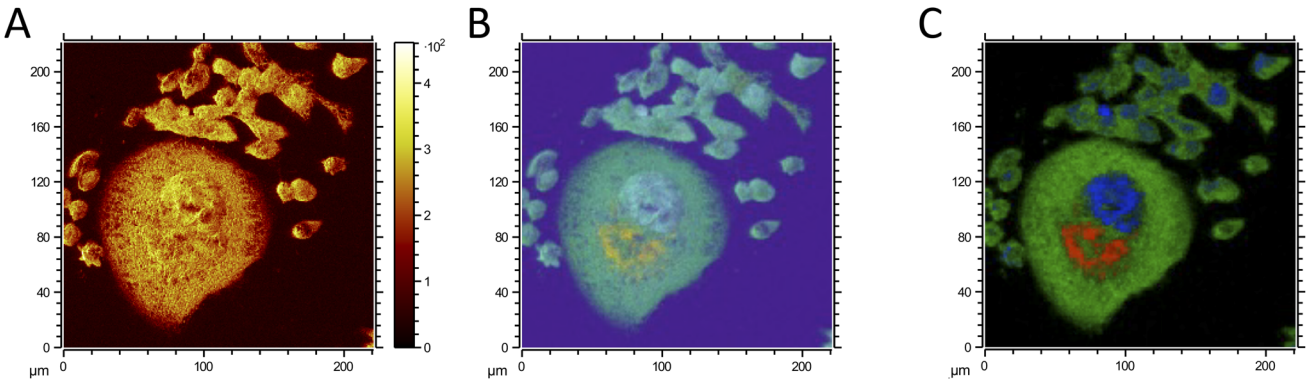

Fig. 8 Negative ion ToF-SIMS images of the mixed sample containing untreated and surviving cancer cells. (A) Total ion image, (B) PCA analysis, and (C) MCR analysis showing the overlay of cytoplasm (red), nucleus (blue), and lipid droplets (red).

cellular oxygen transport. To test this, we measured overall oxygen consumption rates in the large surviving and in the untreated cells. The data demonstrates that the larger cells maintain a high respiration rate (ESI method and result in Fig. S23†). Since a high respiration rate is maintained despite the longer distance for oxygen diffusion in the large surviving cells, this could point towards a role where lipid droplets facilitate faster diffusion. If so, the distribution of lipid droplets may aid these cells in their stress resistance.

In summary, the combined approach of ToF-SIMS and MCR allows us to distinguish intra-cellular regions with increased contents of phosphates, amino acids, lipids, and sulfur. We interpret these regions to likely represent the nucleus (amino acids and phosphates), the remnants of citric metabolism, and lipid droplets. The distribution of droplets of lipids could confer an advantage by facilitating faster diffusion rates of oxygen and maintained aerobic metabolism.

Conclusion

This study provides valuable insights into the chemical alterations that occur in cancer cells as they adapt to survive following cisplatin treatment, specifically through the distribution of lipid droplets. Using ToF-SIMS imaging and multivariate analysis, we successfully detected distinct chemical profiles between untreated and surviving cancer cells. The study highlights the strength of MCR in providing clear separation of cells. These findings have implications for the application of ToF-SIMS in studying cancer biology and understanding chemotherapy resistance. Future research should focus on understanding the precise biochemical pathways involved in lipid droplet formation, their role throughout different stages of the cell cycle, and how this might contribute to increased chemotherapy resistance and cancer cell aggressiveness.

Data availability

The raw data generated and analyzed during this study are openly available from Open Science Framework at **https://osf.io/u2nyk/**

Author contributions

A. Manaprasertsak: conceptualization, data curation, formal analysis, investigation, methodology, visualization, writing – original draft, writing – review and editing. R. Rydbergh formal analysis, methodology, visualization, writing – review and editing. Q. Wu formal analysis, visualization, writing – review and editing. M. Slyusarenko formal analysis, visualization, writing – review and editing. S. Mohlin supervision, methodology, writing – review and editing. S. R Amend supervision, methodology, writing – review and editing. K. J. Pienta: supervision, funding acquisition, methodology, writing – review and editing. P. Malmberg: conceptualization, resources, data curation, formal analysis, supervision, funding acquisition, investigation, methodology, visualization, writing – original draft, writing – review and editing. E. U. Hammarlund: conceptualization, resources, data curation, formal analysis, supervision, funding acquisition, validation, investigation, visualization, methodology, writing – original draft, project administration, writing – review and editing.

Conflicts of interest

There are no conflicts to declare.

Acknowledgements

We thank Chalmers Materials Analysis Laboratory (CMAL) at Chalmers University of Technology for the support with ToF-SIMS experiments. We also thank the Eskil Elmér group Mitochondria Medicine at Lund University and specifically Eleonor Åsander Frostner for helping us with the Seahorse assay. We also thank to TiDE members for their valuable assistance. For funding, we are grateful to the Development and Promotion of Science and Technology Talents Project (DPST), Thailand for the funding support. The authors also thank the Prostate Cancer Foundation (23CHAL11), the Swedish Cancer Society (Pj21 1581), the Sjöberg Foundation, and the Swedish Research Council (2023-03816) for critical funding.

References

1 K. Cilliers, *Clin. Anat.*, 2021, **34**, 766–773.
2 V. Vedam-Mai, J. M. Samuel and B. M. Prentice, *Neural Regener. Res.*, 2024, **19**, 1179–1180.
3 E. J. Ge, A. I. Bush, A. Casini, P. A. Cobine, J. R. Cross, G. M. DeNicola, Q. P. Dou, K. J. Franz, V. M. Gohil and S. Gupta, *Nat. Rev. Cancer*, 2022, **22**, 102–113.
4 F. Larner, *Anal. Bioanal. Chem.*, 2016, **408**, 345–349.
5 I. Tea, E. Martineau, I. Antheaume, J. Lalande, C. Mauve, F. Gilard, S. Barillé-Nion, A. C. Blackburn and G. Tcherkez, *Sci. Rep.*, 2016, **6**, 34251.
6 T. Zuzak, A. Bogaczyk, A. A. Krata, R. Kamiński, P. Paneth and T. Kluz, *Cancers*, 2024, **16**, 3169.
7 A. Manaprasertsak, J. U. Kazi, C. Hagerling, K. J. Pienta, P. Malmberg and E. U. Hammarlund, *Analyst*, 2024, **149**(21), 5344–5352.
8 L. S. Eberlin, X. Liu, C. R. Ferreira, S. Santagata, N. Y. Agar and R. G. Cooks, *Anal. Chem.*, 2011, **83**, 8366–8371.
9 J. Han, H. Permentier, R. Bischoff, G. Groothuis, A. Casini and P. Horvatovich, *TrAC, Trends Anal. Chem.*, 2019, **112**, 13–28.
10 L. Sheng, L. Cai, J. Wang, Z. Li, Y. Mo, S. Zhang, J.-J. Xu, X. Zhang and H.-Y. Chen, *Int. J. Mass Spectrom.*, 2017, **421**, 238–244.
11 I. Kaya, L. S. Schembri, A. Nilsson, R. Shariatgorji, S. Baijnath, X. Zhang, E. Bezard, P. Svenningsson, L. R. Odell and P. E. Andrén, *J. Am. Soc. Mass Spectrom.*, 2023, **34**, 836–846.
12 M. K. Passarelli and N. Winograd, *Biochim. Biophys. Acta, Mol. Cell Biol. Lipids*, 2011, **1811**, 976–990.
13 J. Kałużna-Czaplińska and J. Jóźwik, *TrAC, Trends Anal. Chem.*, 2014, **56**, 1–12.
14 D. Rodrigues, J. Pinto, A. M. Araújo, C. Jerónimo, R. Henrique, M. d. L. Bastos, P. Guedes de Pinho and M. Carvalho, *Metabolites*, 2019, **9**, 18.
15 K. Dimovska Nilsson, N. Neittaanmäki, O. Zaar, T. B. Angerer, J. Paoli and J. S. Fletcher, *Biointerphases*, 2020, **15**(4), 041012.
16 T. B. Angerer, Y. Magnusson, G. r. Landberg and J. S. Fletcher, *Anal. Chem.*, 2016, **88**, 11946–11954.
17 S. K. Gularyan, A. A. Gulin, K. S. Anufrieva, V. O. Shender, M. I. Shakhparonov, S. Bastola, N. V. Antipova, T. F. Kovalenko, Y. P. Rubtsov, Y. A. Latyshev, A. A. Potapov and M. S. Pavlyukov, *Mol. Cell. Proteomics*, 2020, **19**, 960–970.
18 M. H. Philipsen, E. Hansson, A. Manaprasertsak, S. Lange, E. Jennische, H. Carén, K. Gatzinsky, A. Jakola, E. U. Hammarlund and P. Malmberg, *ACS Chem. Neurosci.*, 2023, **14**, 1602–1609.
19 C. Seydoux, J. A. Ezzedine, G. S. Larbi, S. Ravanel, E. Maréchal, J.-P. Barnes and P.-H. Jouneau, *Anal. Chem.*, 2024, **96**(50), 19917–19925.
20 E. J. Lanni, S. S. Rubakhin and J. V. Sweedler, *J. Proteonomics*, 2012, **75**, 5036–5051.
21 E. B. Monroe, S. P. Annangudi, N. G. Hatcher, H. B. Gutstein, S. S. Rubakhin and J. V. Sweedler, *Proteomics*, 2008, **8**, 3746–3754.
22 A. Zavalin, J. Yang and R. Caprioli, *J. Am. Soc. Mass Spectrom.*, 2013, **24**, 1153–1156.
23 D. J. Graham and L. J. Gamble, *Biointerphases*, 2023, **18**(2), 021201.
24 V. Pareek, H. Tian, N. Winograd and S. J. Benkovic, *Science*, 2020, **368**, 283–290.
25 J. Brison, D. S. Benoit, S. Muramoto, M. Robinson, P. S. Stayton and D. G. Castner, *Surf. Interface Anal.*, 2011, **43**, 354–357.
26 C. Kern, A. Scherer, L. Gambs, M. Yuneva, H. Walczak, G. Liccardi, J. Saggau, P. Kreuzaler and M. Rohnke, *Chem.:Methods*, 2024, **4**, e202400008.
27 C. Carroll, A. Manaprasertsak, A. Boffelli Castro, H. van den Bos, D. C. J. Spierings, R. Wardenaar, A. Bukkuri, N. Engström, E. Baratchart, M. Yang, A. Biloglav, C. K. Cornwallis, B. Johansson, C. Hagerling, M. Arsenian-Henriksson, K. Paulsson, S. R. Amend, S. Mohlin, F. Foijer, A. McIntyre, K. J. Pienta and E. U. Hammarlund, *Cancer Res. Commun.*, 2024, **4**, 691–705.
28 K. Pienta, E. Hammarlund, R. Austin, R. Axelrod, J. Brown and S. Amend, *Semin. Cancer Biol.*, 2022, **81**, 145–159.
29 R. Mirzayans, B. Andrais and D. Murray, *Cancers*, 2018, **10**, 118.
30 K. Mittal, S. Donthamsetty, R. Kaur, C. Yang, M. V. Gupta, M. D. Reid, D. H. Choi, P. C. Rida and R. Aneja, *Br. J. Cancer*, 2017, **116**, 1186–1194.
31 L. G. Kostecka, S. Mendez, M. Li, P. Khare, C. Zhang, A. Le, S. R. Amend and K. J. Pienta, *Prostate*, 2024, **84**, 644–655.
32 L. G. Kostecka, K. J. Pienta and S. R. Amend, *Med. Oncol.*, 2021, **38**, 133.
33 L. G. Kostecka, K. J. Pienta and S. R. Amend, *Front. Ecol. Evol.*, 2021, **9**, 660755.
34 S. G. Ostrowski, M. E. Kurczy, T. P. Roddy, N. Winograd and A. G. Ewing, *Anal. Chem.*, 2007, **79**, 3554–3560.
35 R. Vona, E. Iessi and P. Matarrese, *Front. Cell Dev. Biol.*, 2021, **9**, 622908.
36 X. Hua, C. Szymanski, Z. Wang, Y. Zhou, X. Ma, J. Yu, J. Evans, G. Orr, S. Liu and Z. Zhu, *Integr. Biol.*, 2016, **8**, 635–644.
37 A. Seyer, M. Cantiello, J. Bertrand-Michel, V. Roques, M. Nauze, V. Bezirard, X. Collet, D. Touboul, A. Brunelle and C. Comera, *PLoS One*, 2013, **8**, e58224.
38 Q. P. Vanbellingen, N. Elie, M. J. Eller, S. Della-Negra, D. Touboul and A. Brunelle, *Rapid Commun. Mass Spectrom.*, 2015, **29**, 1187–1195.
39 D. Touboul, A. Brunelle, F. Halgand, S. De La Porte and O. Laprévote, *J. Lipid Res.*, 2005, **46**, 1388–1395.
40 Z. Li, S. Cheng, Q. Lin, W. Cao, J. Yang, M. Zhang, A. Shen, W. Zhang, Y. Xia and X. Ma, *Nat. Commun.*, 2021, **12**, 2869.
41 C. Wenbo and T. Jun, *Chin. J. Anal. Chem.*, 2023, **51**, 100290.
42 J. D. Hayes, A. T. Dinkova-Kostova and K. D. Tew, *Cancer Cell*, 2020, **38**, 167–197.
43 M. J. Taylor, K. Y. Zhang, D. J. Graham and L. J. Gamble, *Surf. Sci. Spectra*, 2018, **25**(2), 025001.

44 E. F. Strittmatter, P. D. Schnier, J. S. Klassen and E. R. Williams, *J. Am. Soc. Mass Spectrom.*, 1999, **10**, 1095–1104.
45 N. Samuel and D. Castner, *Appl. Surf. Sci.*, 2004, **231**, 397–401.
46 S. Minchin and J. Lodge, *Essays Biochem.*, 2019, **63**, 433–456.
47 M. Piraud, C. Vianey-Saban, K. Petritis, C. Elfakir, J. P. Steghens, A. Morla and D. Bouchu, *Rapid Commun. Mass Spectrom.*, 2003, **17**, 1297–1311.
48 J. Chen, L. Cui, S. Lu and S. Xu, *Cell Death Dis.*, 2024, **15**, 42.
49 B. Keevil, L. Owen, S. Thornton and J. Kavanagh, *Ann. Clin. Biochem.*, 2005, **42**, 357–363.
50 Y. Wang and C. V. Dang, *Cancer Res.*, 2024, **84**, 2046–2048.
51 N. P. Ward and G. M. DeNicola, *International Review of Cell and Molecular Biology*, 2019, vol. 347, pp. 39–103.
52 W. Szlasa, I. Zendran, A. Zalesińska, M. Tarek and J. Kulbacka, *J. Bioenerg. Biomembr.*, 2020, **52**, 321–342.
53 D. J. Graham and D. G. Castner, *Biointerphases*, 2012, **7**, 49.
54 J. Lee, I. Gilmore and M. Seah, *Surf. Interface Anal.*, 2008, **40**, 1–14.
55 S. Chatterjee, B. Singh, A. Diwan, Z. R. Lee, M. H. Engelhard, J. Terry, H. D. Tolley, N. B. Gallagher and M. R. Linford, *Appl. Surf. Sci.*, 2018, **433**, 994–1017.
56 S. C. Pias, *J. Physiol.*, 2021, **599**, 1769–1782.

